


Pressure dependence of the crystal-field spectrum of KNiF₃: Single and double excitations

J. A. Barreda-Argüeso and F. Rodríguez 

MALTA CONSOLIDER Team, Earth Sciences and Condensed Matter Physics Department (DCITIMAC), Facultad de Ciencias, Universidad de Cantabria, 39005 Santander, Spain



(Received 30 November 2020; revised 20 January 2021; accepted 25 January 2021; published 11 February 2021)

This work investigates the Ni-F distance dependence of the crystal-field (CF) transitions of Ni²⁺ in KNiF₃ by high-pressure spectroscopy. All peaks shift to higher energy with pressure according to trends foreseen by the Tanabe-Sugano diagram. At ambient conditions, we obtain Racah and CF splitting parameters of $B = 0.118$ eV, $10Dq = 0.908$ eV; $C/B = 4.4$ ($10Dq/B = 7.7$). B and $10Dq$ vary with pressure as $\frac{\partial B}{\partial P} = -0.11$ meV GPa⁻¹ and $\frac{\partial 10Dq}{\partial P} = 24$ meV GPa⁻¹. Similar to KCoF₃, the slight decrease of B with pressure reflects the strong ionic character of the Ni-F bond and its high stability against compression. We have correlated the measured pressure dependence of $10Dq$ with the Ni-F bond distance, showing that it follows a potential law as $10Dq = CR^{-n}$ with an exponent $n = 6.6 \pm 0.5$, thus providing experimental data for checking the suitability of theoretical models aiming to explain the slight deviations of observed R dependencies of $10Dq$ from the CF theory ($n = 5$). We have applied the experimental $10Dq(R)$ relationship to determine the real Ni-F bond distances in fluoroperovskites ABF₃: Ni²⁺ from the spectroscopically measured $10Dq$ as an alternative method for determining bond distances, $R_{\text{Ni-F}}$, in impurity systems. We show that the so-obtained $R_{\text{Ni-F}}$ deviates from the bond distance of the host site, R_{B-F} , proportionally to the difference $R_{B-F} - R_0$, with R_0 being the sum of ionic radii $R_{F^-} + R_{\text{Ni}^{2+}}$. The behavior is compared to that found for Mn²⁺ along the fluoroperovskite series ABF₃: Mn²⁺. Finally, weak UV peaks observed below the charge-transfer band gap ($E_g \leq 10$ eV) in the absorption spectrum, the assignment of which still remains controversial, have been assigned to single and double excitation transitions. The assignment was unveiled on the basis of their energy and pressure shift.

DOI: [10.1103/PhysRevB.103.085115](https://doi.org/10.1103/PhysRevB.103.085115)

I. INTRODUCTION

KNiF₃ is an archetype material for establishing correlations between the electronic structure of a transition-metal cation, Ni²⁺, and its crystal structure, i.e., the Ni²⁺-F⁻ bond length. Its perovskite structure (space group $Pm\bar{3}m$ with $a = 4.012$ Å) [1,2], together with its wide pressure stability, makes it attractive to investigate basics aspects related to volume/bond distance dependence of the electronic structure in a highly symmetric environment. As a basic antiferromagnetic material below $T_N = 246$ K, with spins aligned along $\langle 100 \rangle$, KNiF₃ has been probed to study spin dynamics associated with coherent longitudinal oscillations of the antiferromagnetic order parameter induced by impulsive generation of two-magnon modes by femtosecond optical pulses (the so-called femtonanomagnons) [3,4]. Concerning electronic structure, the absorption spectrum of KNiF₃, which is well known since many years ago [5–7], allows us to explore the crystal-field (CF) related excited states of Ni²⁺ in a wide spectral range (0–6 eV) below the charge-transfer band gap of $E_g \approx 10$ eV [5,8,10]. It includes all mainly electric-dipole single excitation (SE) transitions within the $3d^8$ electronic configuration from the $^3A_{2g}(^3F)$ ground state to the manifold $^3\Gamma_i$ and $^1\Gamma_i$ excited states of spin $S = 1$ and 0, respectively; Γ_i refers to O_h irreducible representations. In addition, some

weak absorption peaks appearing below the band gap in the UV range have been assigned either to SE or to double excitation (DE) transitions but their assignment still remains unclear [7,11]. Besides, KNiF₃ has been taken together with other fluoroperovskites KBF₃ as a prototype system to check the suitability of DFT methods to calculate structural properties mainly related to the equation of state and elastic constants [9,10,12–16]. In spite of it, different values of the bulk modulus ranging from 60 to 115 GPa have been recently reported in KNiF₃ [9,10,17,18], showing important discrepancies with the experimental value derived from acoustic measurements of $K_0 = 84$ GPa [18,19]. It shows also important differences with bulk moduli obtained from the experimental $V(P)$ data in isostructural KCoF₃ ($K_0 = 117$ GPa) [20,21], KMnF₃ ($K_0 = 59$ GPa) [22], or KZnF₃ ($K_0 = 78$ GPa) [23]. This dispersion of data points out that precise theoretical methods for determining structural properties in such simple systems are yet to be improved. A study on the crystallographic and elastic properties of KZnF₃ using density functional theory (DFT) based methods using both general-gradient approximation (GGA) and local-density approximation (LDA) exchange correlation functionals, although it provides fair agreement with experimental data, illustrates the dispersion of calculated data depending on the employed functional [13]. In addition, this work tackles the study of the electronic structure of Ni²⁺ introduced as a substitutional impurity in KZnF₃, and what is more challenging, its pressure dependence [13]. Besides difficulties arising to calculate suitable CF energies of Ni²⁺

*Corresponding author: rodriguf@unican.es

as an impurity inside KZnF_3 , it must be noted that the study first requires an adequate structural description of the lattice relaxation around Ni^{2+} , i.e., the NiF_6 octahedron must relax inward with respect to the host ZnF_6 octahedron due to the shorter ionic radius of Ni^{2+} (0.69 Å) than Zn^{2+} (0.74 Å) [24]. If we consider that the Ni-F bond has an intermediate length between that of Zn-F in KZnF_3 ($a = 2 \times R_{\text{Zn-F}} = 4.056$ Å) [25] and Ni-F in KNiF_3 ($a = 2 \times R_{\text{Ni-F}} = 4.012$ Å) [1,2], then the equilibrium Ni-F distance in KZnF_3 would be close to $R_{\text{Ni-F}} = 2.017(11)$ Å.

It is worth noting that most pressure data in impurity systems derived from DFT calculation lack experimental verification. In particular, $\text{KZnF}_3 : \text{Ni}^{2+}$ is an example as structural correlations between the actual Ni-F and the electronic structure is difficult to achieve experimentally. High pressure x-ray diffraction measurements directly provide information on the Zn-F distance [23] but are inadequate to unveil the real Ni-F bond distance even if we deal with x-ray absorption spectroscopy since it is less sensitive to variations of the Ni-F distance at moderate pressures ($P < K_0$) and hard to measure in diluted systems (< 0.1 mol %).

In this work we investigate the pressure dependence of the CF electronic spectra of KNiF_3 in the 0–12-GPa range. The aim is threefold. First, we will provide information on the pressure shifts of the different CF electronic transitions $E(P)$ and correlate it with the variation of the Ni-F distance through the bulk modulus in a pressure range where this perovskite is stable. Second, the $E(R)$ variations enable us to check the suitability of CF models to account for the pressure-induced peak shifts, and to establish structural correlations. In particular, we will be able to estimate the real Ni-F distance, R , in impurity systems $\text{ABF}_3 : \text{Ni}^{2+}$ through the obtained relationship $10Dq = CR^{-n}$. The results will be compared with well-known correlations already established in $\text{ABF}_3 : \text{Mn}^{2+}$ [26,27]. Also, they allow us to compare the experimentally obtained n exponent for KNiF_3 with that obtained for $\text{KZnF}_3 : \text{Ni}^{2+}$ ($n = 6$) from DFT methods [13], which is different from that spectroscopically derived for Mn^{2+} along the $\text{ABF}_3 : \text{Mn}^{2+}$ series ($n = 4.7$) [26,27] or that reported for Co^{2+} in KCoF_3 ($n = 5.1$) through high-pressure measurements [21]. Precise measurements of n are deserving of adequate theoretical methods to explain the slight departure of n from the CF theory estimates of $n = 5$, due to bonding effects related to specificities of the transition-metal cation and the ligand (crystal structure) [13,28,29]. Third, besides SE CF transitions from the $^3A_{2g}(F)$ ground state to the different manifold excited states $^3\Gamma_i$ and $^1\Gamma_i$, concentrated Ni^{2+} compounds may exhibit DE transitions, involving pair excitations as $^3A_{2g}(F)^A + ^3A_{2g}(F)^B \rightarrow ^{3,1}\Gamma_i^A + ^{3,1}\Gamma_j^B$, where A and B refer to nearest-neighbor Ni^{2+} sites, which are activated by the spin-effective electric-dipole mechanism in exchange coupled systems [30–35]. In KNiF_3 , weak absorption features appearing in the UV region above 3.5 eV have been previously assigned either to electric-dipole SE transitions involving states of different spin multiplicity or to DE transitions. In particular, the peak at 3.81 eV ($31\,200\text{ cm}^{-1}$) has been assigned either to the SE $^3A_{2g}(F) \rightarrow ^1E_g(G)$ [7] or to the DE $^3A_{2g}(F)^A + ^3A_{2g}(F)^B \rightarrow ^1E_g(D)^A + ^1E_g(D)^B$ in KNiF_3 [9,29]. Pressure data can clarify such an assignment on the basis of the respective pressure shifts,

since the two band assignments yield different pressure shifts.

II. EXPERIMENT

Float-zone single crystals of KNiF_3 growth by Bridgman were used in present experiments. Its cubic $Pm\bar{3}m$ structure (perovskite phase) is preserved along the explored pressure range. The high-pressure experiments were carried out in a Almax-Boehler Diamond Anvil Cell (DAC) with type IIa diamond anvils of 350 μm culet diameter. 150- μm -thick Inconel gaskets were preindented to 60 μm . 200- μm -diameter holes were perforated with a BETSA motorized electrical discharge machine.

The DAC was loaded with a single crystal (100) plate of KNiF_3 ($100 \times 90 \times 35\text{ }\mu\text{m}$ [3]) and ruby microspheres (5 μm diameter) as pressure probes using silicon oil as pressure-transmitting medium (see Fig. S4 of the Supplemental Material [36]). The pressure was determined from the ruby luminescence following recent revisions on the ruby pressure scale [37].

Optical absorption under high-pressure conditions in the vis-IR range (400–1700 nm) was performed on a prototype fiber-optics microscope equipped with two 25 \times reflecting objectives mounted on two independent x – y – z translational stages for the microfocus beam, and the collector objective and a third independent x – y – z translational stage for the DAC holder. Optical absorption data and images were obtained simultaneously with the same device [38]. Spectra in the visible-infrared (vis-IR) were recorded with Ocean Optics USB 2000 and NIRQUEST 512 monochromators using Si- and InGaAs charge-coupled device detectors, respectively. In the UV range (230–420 nm), we used a reflecting optics spectrophotometer setup. The light of a deuterium lamp was monochromatized by means of Spectra Pro-300i Acton Research Corporation Monochromator and suitable filters. The monochromatic light was chopped and focused with an aluminum-coated toroidal mirror in the diaphragm of a 35 \times reflecting objective, which focused a 10- μm beam spot on the DAC cavity. The transmitted light passed first through the sample (I) and then through the pressure transmitting medium (I_0) was scanned. It was collected with another 35 \times reflecting objective and synchronously detected with a Hamamatsu R-928S phototube and a SR 830 lock-in amplifier. Both reflecting objectives were mounted on two independent x – y – z translational stages for light focusing and light detection. No optical fiber was used in this setup, and the UV lower wavelength limit was imposed by the diamond absorption. The absorption spectra, at ambient conditions and low temperature, were obtained on a Cary 6000 i (Varian) using a (100) single crystal plate of KNiF_3 ($2 \times 2 \times 0.23\text{ mm}^3$).

III. RESULTS AND DISCUSSION

A. Optical absorption spectra and crystal-field analysis

Figure 1 shows the room-temperature (RT) optical absorption spectrum of KNiF_3 with the corresponding peak assignment to electronic CF transitions, the energy of which is well described on the basis of the Tanabe-Sugano diagram for $3d^8$. The assignment and CF parameters are similar to

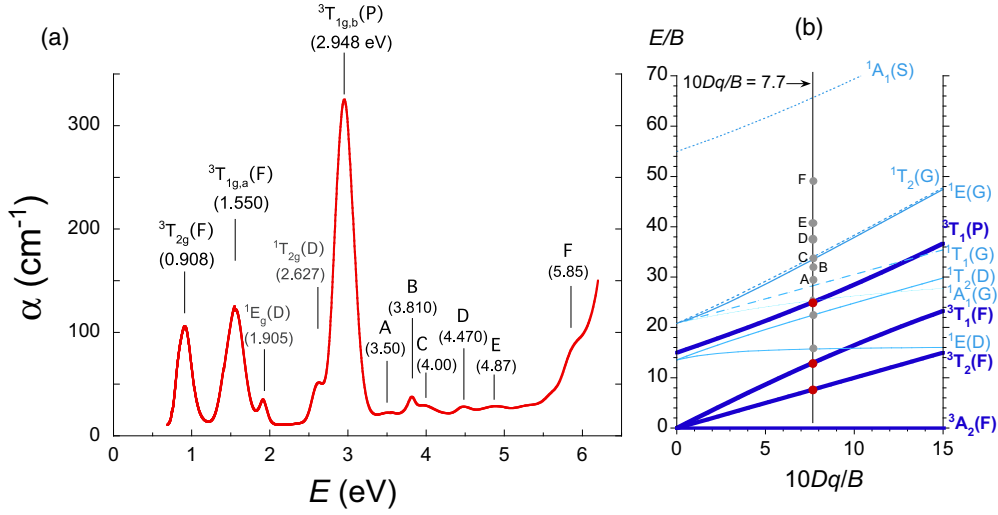


FIG. 1. (a) Room-temperature absorption spectrum of KNiF₃ (space group $Pm\bar{3}m$ with $a = 4.012 \text{ \AA}$). Peak energies and their assignment are indicated. Peaks are assigned to crystal-field transitions from the $^3A_{2g}(F)$ ground state to the $^3\Gamma_1$ i th-excited state, Γ_i being O_h irreducible representations. (b) Tanabe-Sugano diagram for d^8 electronic configuration indicating the crystal-field strength of Ni²⁺ in KNiF₃. The energies of the room-temperature absorption spectrum (dark-blue and azure dots in the Tanabe-Sugano diagram) correspond to $B = 0.118 \text{ eV}$ (950 cm^{-1}), $C/B = 4.4$, and $10Dq = 0.908 \text{ eV}$ (7320 cm^{-1}): $10Dq/B = 7.7$.

those given originally elsewhere [39,40]. The CF parameter $10Dq$ can be directly derived from the first band, $^3A_{2g}(F) \rightarrow ^3T_{2g}(F)$, whose transition energy is $E_1 = 10Dq$. The Racah parameter B can be derived from the energies E_2 and E_3 of the two other spin-allowed transitions $^3A_{2g}(F) \rightarrow ^3T_{1g,a}(F)$ and $^3A_{2g}(F) \rightarrow ^3T_{1g,b}(P)$, respectively, through the equation

$$B = (E_3 + E_2 - 3E_1)/15. \quad (1)$$

Hence the intersect point in the Tanabe-Sugano diagram [28] is given by $10Dq/B = 15E_1/(E_2 + E_3 - 3E_1)$, which is $10Dq/B = 7.7$ at ambient pressure. The Tanabe-Sugano diagram for a d^8 electronic configuration (Ni²⁺) of Fig. 1(b) shows the experimental CF transition energies of the KNiF₃ absorption spectrum and the calculated ones using $B = 0.118 \text{ eV}$, $10Dq = 0.908 \text{ eV}$; $C/B = 4.4$ ($10Dq/B = 7.7$). It must be noted that the C parameter is obtained from the positions of the spin-singlet transition, $^3A_{2g}(F) \rightarrow ^1E_g(D)$, the energy of which depends mainly on both B and C Racah parameters [28]. The obtained B , C , and $10Dq$ values coincide, within the fitting accuracy, to those formerly given elsewhere [38]. The rich peak structure observed in the absorption spectrum corresponds to CF transitions from the $^3A_{2g}(F)$ ground state to different excited states of the same spin multiplicity: $^3T_{2g}(F)$ at 0.908 eV, which corresponds to the energy separation of 3 d orbitals of Ni²⁺ split into $e_g + t_{2g}$ orbitals in the octahedral CF of KNiF₃; $^3T_{1g,a}(F)$ at 1.550 eV; and $^3T_{1g,b}(P)$ at 2.948 eV. Additional weaker peaks at 1.905 and 2.627 eV correspond to electric-dipole transitions to zero-spin excited states $^1E_g(D)$ and $^1T_{2g}(D)$, respectively, whose transition oscillator strength is activated by spin-orbit coupling and exchange mechanism in exchange-coupled Ni²⁺ pairs [40]. Interestingly, there are several bands above 3.4 eV, the assignment of which still remains controversial as they have been assigned either to SE [7] or to DE [11] transitions. Their assignment on the basis of their pressure shifts is given in Sec. III D.

B. High-pressure measurements: Shift rates

Figure 2 shows the variation of the optical absorption spectrum of KNiF₃ with pressure in the 0–12-GPa range. The $Pm\bar{3}m$ perovskite structure is stable in this pressure range, hence the O_h symmetry at the Ni²⁺ site is preserved in the whole pressure range ($a = 2 \times R_{\text{Ni-F}}$). All bands blueshift with pressure with a different pressure coefficient depending on the involved excited state. The transition energy evolution follows the trend foreseen by the Tanabe-Sugano diagram from $10Dq/B = 7.7$ at ambient pressure to $10Dq/B = 9.7$ at 10 GPa, i.e., $10Dq$ increases from 0.908 to 1.150 eV, and B slightly decreases by -1.1 meV from 0.118 to 0.117 eV (Fig. 3). Figure 2 plots the variation of the peak energies with pressure (see also Figs. S1–S3 of the Supplemental Material [36]). We observe that transition energies involving states of the same spin multiplicity follow a linear dependence with pressure in the whole pressure range, whereas those associated with spin change ($S = 1 \rightarrow 0$) transitions exhibit an additional small quadratic dependence above about 7 GPa that can be attributed to their strong overlap with the more intense peaks (Fig. 2 and Fig. S2 of the Supplemental Material [36]). The least-squares linear fit equations for each transition are given in Fig. 2(b). Unfortunately, the small peaks appearing above 4.2 eV could not be measured as a function of pressure because of their large overlap. Only the small narrow features at 3.47 and 3.81 eV were detected up to 12 and 3 GPa, respectively. Peak shifts, overlap, and diamond absorption impede a proper detection of the remainder of higher energy peaks (Fig. 2). Interestingly, both the peak energies and their pressure coefficients agree fairly well with trends of the Tanabe-Sugano diagram as it is shown in Fig. 1(b) and Table I. It must be noted that the observed blueshift of the almost $10Dq$ -independent $^1E_g(D)$ at 1.916 eV is 1.3 meV GPa^{-1} in agreement with the slight $10Dq$ dependence of this spin-flip transition as $\frac{\partial E[^1E_g(D)]}{\partial 10Dq} = 0.06$, i.e.,

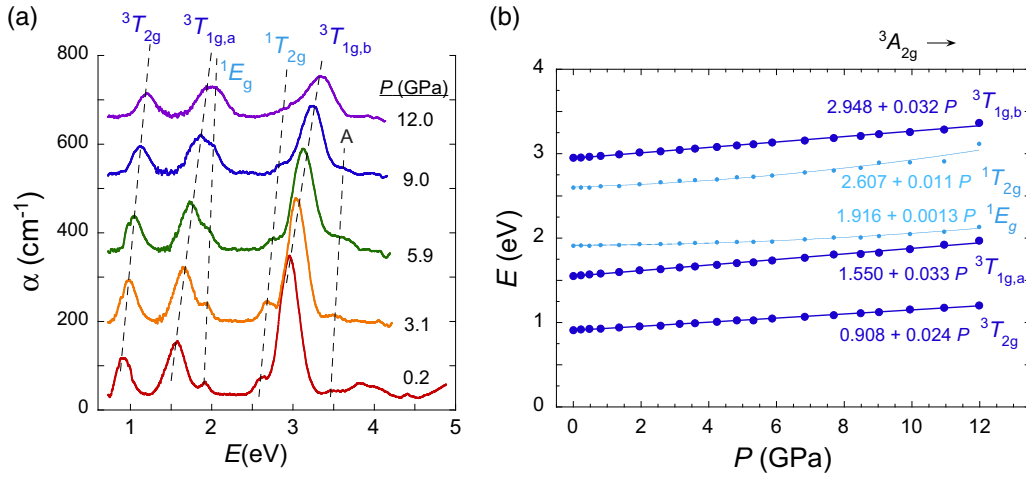


FIG. 2. (a) Pressure dependence of the absorption spectrum of KNiF₃ in the 0–12-GPa range. Dashed lines are eye guides to illustrate the different pressure shift of each peak. (b) Variation of the peak energy with pressure. The corresponding least-square linear fit equations are given on the right side. Data are collected in Table I (more details in Figs. S1–S3 of the Supplemental Material [36]).

$\frac{\partial E[{}^1E_g(D)]}{\partial P} = 1.4 \text{ meV GPa}^{-1}$ (Table I). The accuracy of this method is worthwhile to predict the pressure coefficient for those peaks whose pressure coefficients could not be measured due to experimental impediments.

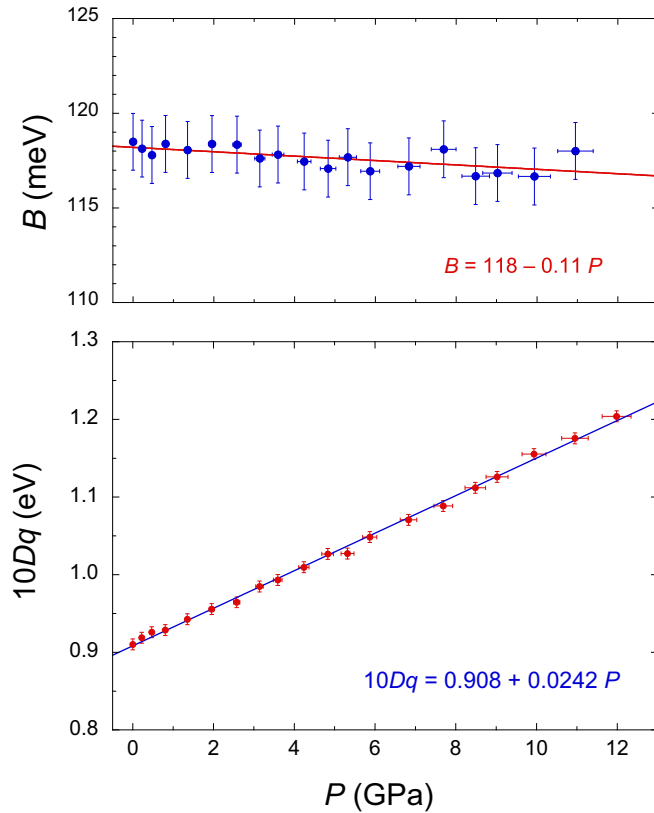


FIG. 3. Variation of the (a) crystal-field splitting $10Dq$ and (b) Racah parameter B with pressure in KNiF₃. Straight lines correspond to the least-square fits of the experimental data to the linear equation: $10Dq = 10Dq_0 + \frac{\partial 10Dq}{\partial P}P$ and $B = B_0 + \frac{\partial B}{\partial P}P$.

C. $10Dq$ dependence on the Ni-F distance: Bond distance estimates in Ni²⁺ impurities

The present spectroscopic results enable us to determine the $10Dq$ dependence on $R_{\text{Ni-F}}$ from the KNiF₃ bulk modulus $K_0 = 84(1) \text{ GPa}$, derived from acoustic measurements [18,19], and compare it with those obtained by DFT methods [9,14,15,17]. On the basis of potential law dependence of $10Dq$ with $R_{\text{Ni-F}}$ as $10Dq = CR_{\text{Ni-F}}^{-n}$, we can obtain the exponent of this potential law from the pressure dependence of $10Dq$:

$$\left(\frac{\partial 10Dq}{\partial P}\right)_T = \left(\frac{\partial 10Dq}{\partial R_{\text{Ni-F}}}\right)\left(\frac{\partial R_{\text{Ni-F}}}{\partial P}\right)_T = \frac{n}{3K_0} 10Dq. \quad (2)$$

Taking the measured pressure shift coefficient, $\left(\frac{\partial 10Dq}{\partial P}\right)_T = 24 \text{ meV GPa}^{-1}$, and the ambient pressure values of the bulk modulus and $10Dq$, we obtain $n = 6.6 \pm 0.5$. Interestingly, the exponent n is larger than the exponent $n = 5$ predicted by the CF theory [28], and its difference must be ascribed to changes of the actual molecular-orbital wave function with R (bonding), which modulates the dependence of $10Dq(R)$ yielding a potential law proportional to R^{-n} with $n = 6.6$ in KNiF₃. Previous works exploring the R dependence of $10Dq$ in the ABF_3 : Mn²⁺ perovskite series [26] and in Co²⁺ in the isostructural KCoF₃ ($Pm\bar{3}m$) [21] provide potential law dependencies with n exponents of 4.7 and 5.1, respectively. Though in all cases exponents are around 5, their departures from $n = 5$ unveil singularities which are related to the different nature of the lattice and the bonding between the transition-metal ion and the ligand. The present results provide experimental data that can be fundamental to probe the suitability of theoretical calculation methods to account for such n deviations. Previous DFT-based methods employed to explore pressure dependencies in KZnF₃: Ni²⁺ using LDA and GGA functionals provide an adequate methodology to face this problem [13]. However, the results of such calculations could not be checked due to the lack of high-pressure measurement in Ni²⁺ diluted systems. The present work on KNiF₃ provides experimental evidence for such estimates. In

TABLE I. Transition energies and associated Racah (B , C) and crystal-field splitting $10Dq$ parameters of Ni^{2+} in KNiF_3 , obtained from the optical absorption spectrum at ambient pressure and 10 GPa. The energies of the main crystal-field transitions are represented in the Tanabe-Sugano diagram for $d^8(O_h)$ in Fig. 1. The calculated transition energy E and its pressure derivative with respect to $10Dq$, $\frac{\partial E}{\partial 10Dq}$, of each absorption peak, obtained from the slope of the $E/B(10Dq/B)$ curve of the Tanabe-Sugano diagram at $10Dq/B = 7.7$, are included. The calculated pressure coefficients have been obtained from $\frac{\partial E}{\partial 10Dq}$ times the measured $\frac{\partial 10Dq}{\partial P}$ coefficient. Pressure dependences of B and $10Dq$ in KNiF_3 are $\frac{\partial 10Dq}{\partial P} = 24.2 \text{ meV GPa}^{-1}$, $\frac{\partial B}{\partial P} = -0.11 \text{ meV GPa}^{-1}$ (Fig. 3). The ratio C/B is fixed to 4.4 with pressure consistently with experimental data.

	Peak assignment: ${}^3A_{2g}(F) \rightarrow$							
	${}^3T_{2g}(F)$	${}^3T_{1g,a}(F)$	${}^1E_g(D)$	${}^1T_{2g}(D)$	${}^3T_{1g,b}(P)$	${}^1A_{1g}(G)$	${}^1T_{1g}(G)$	${}^1T_{2g}, {}^1E_g(G)$
Expt. E (eV)	0.908	1.550	1.916	2.607	2.948		3.50 (A)	4.00 (C)
Calc. E (eV)	0.908	1.54	1.86	2.66	2.937	3.01	3.36	3.96, 4.03
Expt. $\frac{\partial E}{\partial P}$ (meV GPa $^{-1}$)	24.2	33	1.3	11	32		22	
Calc. $\frac{\partial E}{\partial 10Dq}$	1.00	1.53	0.06	1.03	1.47	0.07	0.97	1.86
Calc. $\frac{\partial E}{\partial P}$ (meV GPa $^{-1}$)	24.2	37	1.4	24	35	1.7	23	45
Pressure Crystal-field parameters ($C/B = 4.4$)								
	0.0001 GPa	$B = 0.118 \text{ eV}$	$10Dq/B = 7.7$					
	10 GPa	$B = 0.117 \text{ eV}$	$10Dq/B = 9.8$					

particular, the theoretical estimates for $\text{KZnF}_3 : \text{Ni}^{2+}$ provide n exponents for the variation of $10Dq$ with $R_{\text{Ni-F}}$ of $n = 5.402$ and 6.016 using GGA and LDA calculations, respectively. The LDA calculation provides a similar exponent to the experimental one measured herein for KNiF_3 ($n = 6.6$) and thus points out the suitability of LDA calculations to describe better pressure dependencies of $10Dq$ than GGA calculations in this perovskite system [13].

The $10Dq(R)$ relationship obtained from high-pressure measurements in KNiF_3 can be applied to determine the $\text{Ni}^{2+}-\text{F}^-$ distance in $\text{ABF}_3 : \text{Ni}^{2+}$ perovskites from $10Dq$ on the assumption that such potential law applies along the perovskite series ABF_3 . First, it must be noted that the variation of $10Dq$ with the B -F host distance, R_{B-F} , along the series [Fig. 4(a)] shows a linear dependence, which is consistent with a potential law as $R_{B-F} = R_0(10Dq_0/10Dq)^{1/n}$, with an exponent $n = 1.2$ for $\text{ABF}_3 : \text{Ni}^{2+}$, quite far from the expected CF value $n \approx 5$. A similar situation occurs in $\text{ABF}_3 : \text{Mn}^{2+}$ where $n = 1.4$ [Fig. 4(a)]. It was shown that this anomalous exponent is caused by the distinct R_{B-F} and $R_{\text{Mn-F}}$, of the host and the impurity, respectively, due to local relaxation effects of the F^- octahedron around the Mn^{2+} impurity [26,27]. The real Mn-F distance $R_{\text{Mn-F}}$ is intermediate between that of the host R_{B-F} and the sum of the Mn^{2+} and F^- ionic radii, $R_0 = R_{\text{Mn}^{2+}} + R_{\text{F}^-} = 2.107 \text{ \AA}$ [24]. Here we assume that a similar situation is attained in $\text{ABF}_3 : \text{Ni}^{2+}$. Table II collects structural and spectroscopic data for $\text{ABF}_3 : \text{Ni}^{2+}$ with Ni-F distance estimates derived from the measured $10Dq$ on the basis of the potential law $R_{\text{Ni-F}} = R_0(10Dq_0/10Dq)^{1/6.6}$ with $R_0 = 2.006 \text{ \AA}$ and $10Dq_0 = 0.908 \text{ eV}$ (ambient pressure data) experimentally obtained in KNiF_3 using high-pressure spectroscopy. Figure 4(b) shows the variation of the $10Dq$ -derived M -F distance, R_{10Dq} , as a function of the host B -F distance for both $M : \text{Mn}^{2+}$ and Ni^{2+} . Interestingly, both variations show that the actual M -F bond distance corresponds neither to R_{B-F} nor to R_0 but to an intermediate value which amounts to about 20–30% of the departure of R_{B-F} from R_0 . Therefore, when M is introduced as a substitutional impurity at the octahedral BF_6 site, an outward or inward relaxation of the F^-

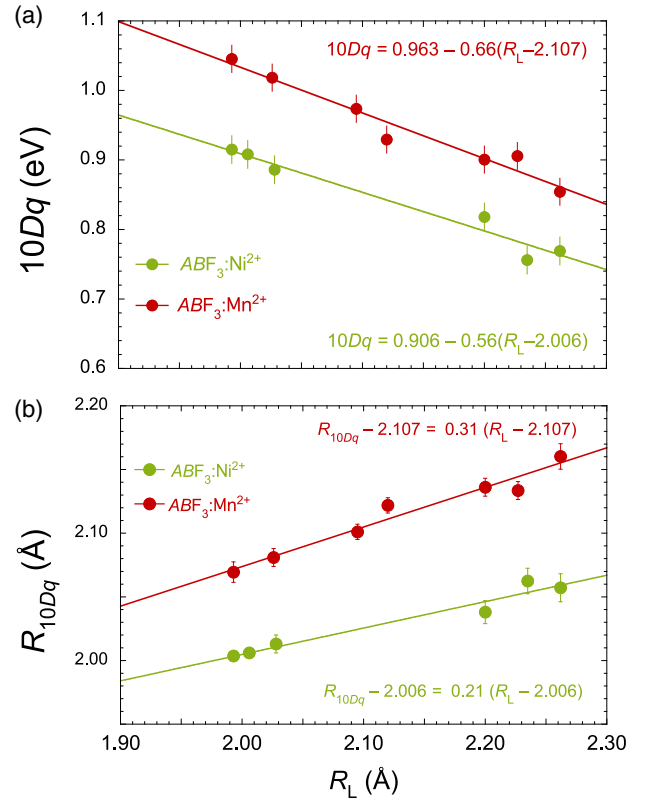


FIG. 4. (a) Variation of the crystal-field splitting $10Dq$ with the host B -F distance, R_L , along the $\text{ABF}_3 : M^{2+}$ fluoroperovskite series for $M : \text{Mn}^{2+}$ and Ni^{2+} . The straight lines are the least-square fit of the experimental data to the linear equation: $10Dq = 10Dq_0 + \frac{\partial 10Dq}{\partial R_L}(R_L - R_0)$. The pressure coefficients $\frac{\partial 10Dq}{\partial R_L} = -0.66$ and $-0.56 \text{ eV \AA}^{-1}$ for Mn^{2+} and Ni^{2+} , respectively, correspond to n exponents of the potential law $R_L = R_0(\frac{10Dq_0}{10Dq})^{1/n}$ of 1.4 and 1.2, respectively. (b) Variation of the M -F distance derived from $10Dq$ through the equation $R_{10Dq} = R_0(\frac{10Dq_0}{10Dq})^{1/n}$, using $R_0 = 2.107 \text{ \AA}$; $10Dq_0 = 0.963 \text{ eV}$; and $n = 4.7$ for $M : \text{Mn}^{2+}$ [26,27], and $R_0 = 2.006 \text{ \AA}$; $10Dq_0 = 0.908 \text{ eV}$; and $n = 6.6$ for $M : \text{Ni}^{2+}$. Experimental plotted data are collected in Table II.

TABLE II. Variation of the B - F distance, R_L , along the host ABF_3 : M^{2+} perovskite series and crystal-field parameter $10Dq$ for M : Mn^{2+} and Ni^{2+} . The M - F distance has been derived from the measured $10Dq$ at room temperature through the equation $R_{10Dq} = R_0(\frac{10Dq_0}{10Dq})^{1/n}$, using $R_0 = 2.107 \text{ Å}$, $10Dq_0 = 0.963 \text{ eV}$, and $n = 4.7$ for M : Mn^{2+} [26,27], and $R_0 = 2.006 \text{ Å}$, $10Dq_0 = 0.908 \text{ eV}$, and $n = 6.6$ for M : Ni^{2+} . Errors in R_{10Dq} are given in parentheses.

Compound	R_L (Å) $\pm 0.001 \text{ Å}$	$10Dq$ (eV) $\pm 0.007 \text{ eV}$	R_{10Dq} (Å) (standard deviation in parentheses)	Ref.
KMgF ₃ : Mn^{2+}	1.993	1.045	2.069(8)	
KZnF ₃ : Mn^{2+}	2.026	1.018	2.081(7)	
KMnF ₃	2.095	0.974	2.101(6)	
RbMnF ₃	2.120	0.929	2.122(6)	[26,27]
RbCdF ₃ : Mn^{2+}	2.200	0.901	2.134(7)	
RbCaF ₃ : Mn^{2+}	2.227	0.906	2.131(7)	
CsCaF ₃ : Mn^{2+}	2.262	0.854	2.160(10)	
KMgF ₃ : Ni^{2+}	1.993	0.915	2.004(3)	[5,39,40]
KNiF ₃	2.006	0.908	2.006(3)	[5,39,40], this work
KZnF ₃ : Ni^{2+}	2.028	0.886	2.013(7)	[41]
RbCdF ₃ : Ni^{2+}	2.200	0.818	2.038(9)	[42]
CsCdF ₃ : Ni^{2+}	2.235	0.756	2.063(11)	[43,44]
CsCaF ₃ : Ni^{2+}	2.262	0.769	2.057(11)	[43] ^a

^aDue to the lack of room-temperature absorption spectrum of CsCaF₃ : Ni^{2+} , its $10Dq$ was obtained by adding 0.013 eV to the $10Dq$ value of CsCdF₃ : Ni^{2+} . This shift corresponds to the energy difference of the corresponding $^3T_{2g}(F) \rightarrow ^3A_{2g}(F)$ emission zero-phonon lines at 10 K : $E_{ZPL}(\text{CsCaF}_3 : \text{Ni}^{2+}) - E_{ZPL}(\text{CsCdF}_3 : \text{Ni}^{2+})$.

octahedron takes place depending on whether R_{B-F} is shorter or longer than 2.006 Å (or 2.107 Å) for Ni^{2+} (or Mn^{2+}), respectively.

D. Double excitation versus single excitation transitions of UV bands

The absorption spectrum of KNiF₃ shows at least six weak absorption peaks between 3.4 and 6 eV, named A–F, the origin of which is still controversial (Fig. 1). The three peaks appearing together around 3.81 eV (namely A–C) were assigned to SE transitions $^3A_{2g}(F) \rightarrow ^1T_{1g}(G)$, $^1E_g(G)$, and $^1T_{2g}(G)$ [7], whereas two of them were assigned to DE transitions $^3A_{2g}(F)^A + ^3A_{2g}(F)^B \rightarrow ^1E_g(D)^A + ^1E_g(D)^B$ [11]. Their transition energy is close to predictions of the Tanabe-Sugano diagram in the former case (Fig. 1) but also to twice the SE $^1E_g(D)$ energy ($2 \times 1.905 = 3.81 \text{ eV}$) in the latter one, or even other combinations as $^3T_{2g}(F)^A + ^3T_{1g}(P)^B$ with an energy of 3.856 eV (Fig. 1). The DE assignment was based on the fact that the band intensity (oscillator strength f) depends strongly on the Ni^{2+} concentration in $K(\text{Mg}_{1-x}\text{Ni}_x)\text{F}_3$ (f increases by an order of magnitude from $x = 0.1$ to 1), thus clearly indicating that such transitions are associated with the number Ni-F-Ni pairs—exchange-coupled pair transition [40]. However, it must be noted that not only DE but also SE can be partially activated by the exchange mechanism as well, although the main driving electric-dipole mechanism in SE transitions is the vibronic coupling to odd-parity modes [5]. The point is that the energy of a DE transition is close to the sum of the involved SE transition energies. For a DE such as $^3A_{2g}(F)^A + ^3A_{2g}(F)^B \rightarrow \Gamma_i^A + \Gamma_j^B$, its energy is given by

$$E(\Gamma_i^A + \Gamma_j^B) = E(\Gamma_i^A) + E(\Gamma_j^B) - E_{\text{exch}} \approx E(\Gamma_i^A) + E(\Gamma_j^B), \quad (3)$$

where E_{exch} is the stabilization exchange energy and, in ionic systems, is much smaller than the individual SE energies (less than about 1%) [32–35]. In general, this condition must be fulfilled by all DE transitions. Interestingly, this relationship also applies to the pressure coefficient of DE, and thus makes it a very powerful tool to definitely verify which excited states are involved in a DE transition. In particular, its pressure dependence is given by

$$\begin{aligned} \frac{\partial E(\Gamma_i^A + \Gamma_j^B)}{\partial P} &= \frac{\partial E(\Gamma_i^A)}{\partial P} + \frac{\partial E(\Gamma_j^B)}{\partial P} - \frac{\partial E_{\text{exch}}}{\partial P} \\ &\approx \frac{\partial E(\Gamma_i^A)}{\partial P} + \frac{\partial E(\Gamma_j^B)}{\partial P}. \end{aligned} \quad (4)$$

According to this, a DE transition involving two identical SE ($\Gamma_i = \Gamma_j = ^1E_g(D)$) should have a pressure coefficient nearly twice the SE pressure coefficient. Therefore, a DE assigned to $^1E_g(D)^A + ^1E_g(D)^B$ should have a pressure coefficient of about 3 meV GPa^{−1} (Fig. 2 and Table I, and Figs. S1–S3 of the Supplemental Material [36]).

Figure 5(a) shows the variation of the absorption spectrum with pressure to illustrate the pressure dependence of the 3.48 eV (A) and 3.81 (B) peaks in comparison to the $^1T_{2g}(D)$ and $^3T_{1g}(P)$ SE peaks. The corresponding $E(P)$ variations are given in Fig. 5(b) in the 0–10- and 0–3-GPa range, respectively. Their pressure coefficient of 22 and 9 meV GPa^{−1}, respectively, allows us to unambiguously assign such transitions as the SE $^1T_{1g}(G)$ and the DE $^1E_g(D)^A + ^1E_g(D)^B$, respectively. In the former case, both the energy and pressure coefficient are close to the expected one for the SE $^3T_{1g}(P)$ of 3.36 eV and 23 meV GPa^{−1} [Fig. 1(a) and Table I]. For the 3.81-eV peak, the assignment to a SE transition must be ruled out as its pressure coefficient is too low as compared with those of the $^3T_{1g}(P)$, and $^1T_{2g}(G)$ or $E_g(G)$ SE transitions of 23 and 45 meV GPa^{−1}, respectively. However, its slight pressure

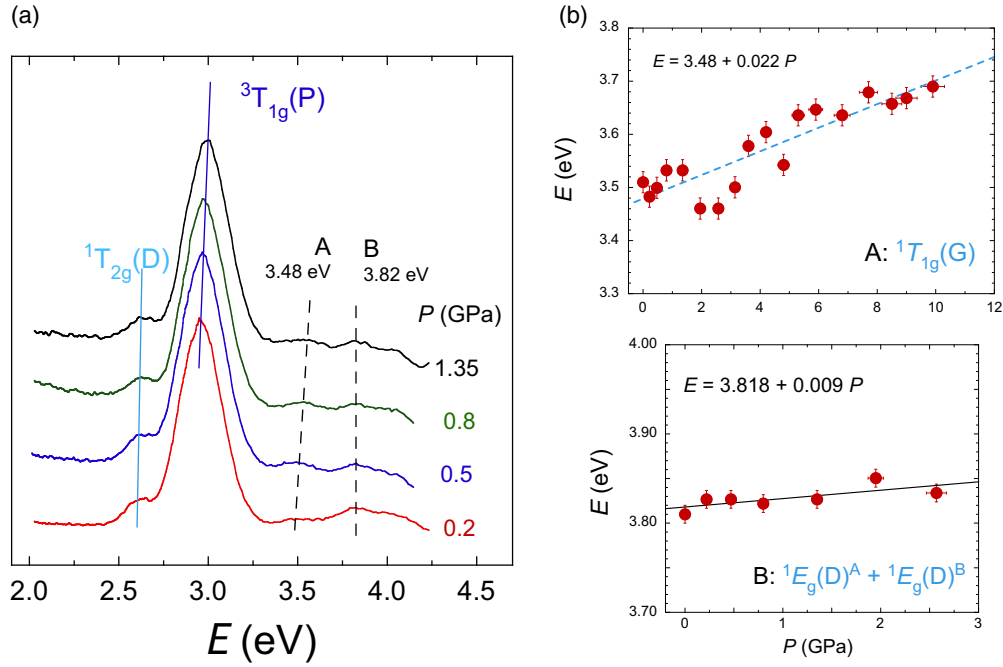


FIG. 5. (a) Variation of the absorption spectrum of KNiF_3 in the UV region in the 1–1.5-GPa range. (b) Energy pressure dependence of the peaks A (3.46 eV) and B (3.81 eV) of KNiF_3 in the range 0–10 and 0–3 GPa, respectively. The straight lines are the least-square fit of the experimental data to a linear equation. Note that both the energy and the pressure coefficient of A and B peaks are slightly close to the sum of the energy and pressure coefficient of the ${}^3T_{1g}(P)$ SE and the ${}^1E_g(D)^A + {}^1E_g(D)^B$ DE transition, respectively.

coefficient is closer to that of the DE ${}^1E_g(D)^A + {}^1E_g(D)^B$ of 3 meV GPa^{-1} , thus confirming the assignment given elsewhere [11].

Though we missed measurements of the pressure coefficients of the higher energy peaks ($>4 \text{ eV}$), named C–F in Fig. 1(a), we must rule out an assignment to SE transitions with the exception of the C peak (4.00 eV) whose energy is close to the overlapping ${}^1T_{2g}(G)$ and ${}^1E_g(G)$ energies of 3.92 and 3.99 eV, respectively [Fig. 1(b)]. On the basis of their transition energy, we tentatively assign peaks D–F to the DE transitions: ${}^1E_g(D)^A + {}^1T_{2g}(D)^B$; ${}^1E_g(D)^A + {}^1A_{1g}(G)^B$; and ${}^1E_g(D)^A + {}^1T_{1g}(G)^B$, respectively (Table I). The reasons are threefold. (i) The peak positions do not correspond to any SE transition in the Tanabe-Sugano diagram. Actually, there is no CF SE in KNiF_3 to account for the observed transitions. (ii) Peaks D (4.47 eV), E (4.87 eV), and F (5.85 eV) fairly agree with the sum of the corresponding SE energies involved in the DE transition: 4.54, 4.87, 5.91 eV, respectively. The slight mismatch would correspond to the exchange stabilization energy of the $\text{Ni}^{2+}\text{—F}^-\text{—Ni}^{2+}$ pair. (iii) All DE transitions involved the almost $10Dq$ -independent spin-flip SE ${}^1E_g(D)$. The involvement of this excited state makes the full width at half maximum (FWHM) of the DE peak be of the order as the SE FWHM thus making its detection easier in the absorption spectrum. Although other combinations for DE transitions involving spin-triplet ${}^3T_{1,2}$ excited states are possible, such possibility is unlikely since the FWHM would amount to twice the SE FWHMs. Moreover, the transition oscillator strength, which is fully concentrated in the only excited state of the pair ($S = 0$) for a DE involving only spin singlet SE ($S = 0$), would spread over the different DE spin

states ($S = 0, 1, 2$) if spin triplet SE states were involved in the DE.

IV. CONCLUSIONS

We have shown that the pressure dependence of the CF transitions of Ni^{2+} in KNiF_3 all shift to higher energy following the trends of the Tanabe Sugano diagram that was calculated using $B = 0.118 \text{ eV}$, $10Dq = 0.908 \text{ eV}$; $C/B = 4.4$ ($10Dq/B = 7.7$) at ambient conditions, B and $10Dq$ varying with pressure as $\frac{\partial B}{\partial P} = -0.11 \text{ meV GPa}^{-1}$ and $\frac{\partial 10Dq}{\partial P} = 24 \text{ meV GPa}^{-1}$. The slight pressure decrease of B reflects the strong ionic Ni-F bond, similar to that of the Co-F bond in KCoF_3 ($\frac{\partial B}{\partial P} = -0.07 \text{ meV GPa}^{-1}$) [21], in comparison to the more covalent $\text{Co}^{2+}\text{—Cl}^-$ or $\text{Mn}^{2+}\text{—Cl}^-$ bonds (both $\frac{\partial B}{\partial P} = -0.3 \text{ meV GPa}^{-1}$) measured in CoCl_2 [45] and $[(\text{CH}_3)_4\text{N}]\text{MnCl}_3$ [46]. We have shown that the variation of $10Dq$ with the Ni-F bond distance R follows a potential law as $10Dq = CR^{-n}$ with an exponent $n = 6.6 \pm 0.5$. This exponent is similar to that obtained for Ni^{2+} in KZnF_3 ($n = 6.016$) from GGA calculations, although no experimental validation was done due to the lack of high-pressure absorption measurements in such a compound. The present results provide suitable data for checking theoretical calculations devoted to explain the deviations of the n exponent of the R dependence of $10Dq$ as R^{-n} from $n = 5$.

We have demonstrated that the measured $10Dq(R)$ relationship in KNiF_3 provides an alternative method to estimate Ni-F bond distances in the $\text{ABF}_3 : \text{Ni}^{2+}$ fluoroperovskite series from the CF splitting $10Dq$ obtained by optical spectroscopy. The so-obtained $R_{\text{Ni—F}}$ bond length deviates from the host

site R_{B-F} one proportionally to the difference $R_{B-F} - R_0$, in such a way that the F^- octahedron around the Ni^{2+} impurity experiences an inward or an outward relaxation of about 21% of the R_{B-F} deviation with respect to $R_0 = 2.006 \text{ \AA}$. This result is very similar to that found for Mn^{2+} impurities (31%) in the $ABF_3 : Mn^{2+}$ fluoroperovskite series [26,27].

Finally, we have demonstrated that the weak UV peaks observed in the optical absorption spectrum of $KNiF_3$, with the exception of the SE A and C, mainly correspond to DE rather than SE transitions. The assignment was done on the basis of both their peak energy as a sum of the two SEs involved in the

DE transition, as well as their corresponding pressure shifts. The latter procedure allows us to correct previous assignments to SE transitions given previously to the 3.81-eV peak B. We have also shown that the assignment of the UV peaks D, E, and F as DE transitions involving spin-flip excited states ($S = 0$) is likely.

ACKNOWLEDGMENTS

Financial support from Projects PGC2018-101464-B-I00 and MALTA-Consolider Team RED2018-102612-T (Ministerio de Ciencia, Innovación y Universidades) is acknowledged.

- [1] K. Knox, *Acta Crystallogr.* **14**, 583(1961).
- [2] N. Kijima and K. Tanaka, *Acta Crystallogr., Sect. B: Struct. Sci.* **39**, 557 (1983).
- [3] D. Bossini, S. Dal Conte, Y. Hashimoto, A. Secchi, R. V. Pisarev, Th. Rasing, G. Cerullo, and A. V. Kimel, *Nat. Commun.* **7**, 10645 (2016).
- [4] D. Bossini, S. Dal Conte, G. Cerullo, O. Gomonay, R. V. Pisarev, M. Borovsak, D. Mihailovic, J. Sinova, J. H. Mentink, Th. Rasing, and A. V. Kimel, *Phys. Rev. B* **100**, 024428 (2019).
- [5] K. Knox, R. G. Shulman, and S. Sugano, *Phys. Rev.* **130**, 512 (1963).
- [6] R. V. Pisarev and S. D. Prochorova, *Phys. Lett.* **26**, 356 (1968).
- [7] N. Mironova, V. Skvortsova, A. Kuzmin, I. Sildos, and N. Zazubovich, in *Defects and Surface-Induced Effects in Advanced Perovskites*, edited by G. Borstel, A. Krumins, and D. Millers (Springer, Dordrecht, 2000), pp. 155–160.
- [8] J. H. Beaumont, A. J. Bourdillon, and J. Bordas, *J. Phys. C: Solid State Phys.* **10**, 333 (1977).
- [9] J. M. Ricart, R. Dovesi, C. Roetti, and V. R. Saunders, *Phys. Rev. B* **52**, 2381 (1995).
- [10] F. Sihem and H. Noura, *Am. J. Mod. Phys. Appl.* **5**, 97 (2018).
- [11] T. Bandai, H. Fukutani, and G. Kuwabara, *Solid State Commun.* **21**, 857 (1977).
- [12] G. Vaitheeswaran, V. Kanchana, R. S. Kumar, A. L. Cornelius, M. F. Nicol, A. Svane, A. Delin, and B. Johansson, *Phys. Rev. B* **76**, 014107 (2007).
- [13] M. G. Brik, G. A. Kumar, and D. K. Sardar, *Mater. Chem. Phys.* **136**, 90 (2012).
- [14] C. De Nadaï, A. Demourgues, J. Grannec, and F. M. F. de Groot, *Phys. Rev. B* **63**, 125123 (2001).
- [15] Hayatullah, G. Murtaza, R. Khenata, S. Muhammad, A. H. Reshak, K. M. Wong, S. Binomran, and Z. Alahmed, *Comput. Mater. Sci.* **85**, 402 (2014).
- [16] Y.-C. Wang and H. Jiang, *J. Chem. Phys.* **150**, 154116 (2019).
- [17] S. Filalli and N. Hamdad, *Annals of West University of Timisoara - Physics* **62**, 23 (2020).
- [18] M. Rousseau, J. Nouet, and A. Zarembovitch, *J. Phys. Chem. Solids* **35**, 921 (1974).
- [19] F. Ganot, C. Dugautier, P. Moch, and J. Nouet, *J. Phys. C: Solid State Phys.* **15**, 801 (1982).
- [20] F. Aguado, F. Rodríguez, and S. A. T. Redfern, *High Press. Res.* **29**, 525 (2009).
- [21] J. A. Barreda-Argüeso, F. Aguado, J. González, R. Valiente, L. Nataf, M. N. Sanz-Ortiz, and F. Rodríguez, *J. Phys. Chem. C* **120**, 18788 (2016).
- [22] S. Aoyagi, S. Toda, E. Nishibori, Y. Kuroiwa, Y. Ohishi, M. Takata, and M. Sakata, *Phys. Rev. B* **78**, 224102 (2008).
- [23] F. Aguado, F. Rodríguez, S. Hirai, J. N. Walsh, A. Lennie, and S. A. T. Redfern, *High Press. Res.* **28**, 539 (2008).
- [24] R. D. Shannon, *Acta Crystallogr., Sect. A: Cryst. Phys., Diffraction, Gen. Crystallogr.* **32**, 751 (1976).
- [25] R. H. Buttner and E. N. Maslen, *Acta Crystallogr., Sect. C: Cryst. Struct. Commun.* **44**, 1707 (1988).
- [26] F. Rodríguez and M. Moreno, *J. Chem. Phys.* **84**, 692 (1986).
- [27] M. C. Marco de Lucas, F. Rodríguez, and M. Moreno, *J. Phys.: Condens. Matter* **5**, 1437 (1993).
- [28] S. Sugano, Y. Tanabe, and H. Kamimura, *Multiplets of Transition-Metal Ions in Crystals* (Academic, New York, 1970).
- [29] A. Trueba, P. Garcia-Fernandez, J. Maria Garcia-Lastra, J. A. Aramburu, M. T. Barriuso, and M. Moreno, *J. Phys. Chem. A* **115**, 1423 (2011).
- [30] J. Ferguson, H. J. Guggenheim, and Y. Tanabe, *J. Phys. Soc. Jpn.* **21**, 692 (1966).
- [31] J. Ferguson, *Aust. J. Chem.* **21**, 323 (1968).
- [32] S. E. Stokowski, D. D. Sell, and H. J. Guggenheim, *Phys. Rev. B* **4**, 3141 (1971).
- [33] T. Fujiwara, W. Gebhardt, K. Petanides, and Y. Tanabe, *J. Phys. Soc. Jpn.* **33**, 39 (1972).
- [34] H. U. Güdel, *Comments Inorg. Chem.* **3**, 189 (1984).
- [35] F. Rodríguez, D. Hernández, and H. U. Güdel, *Phys. Rev. B* **60**, 10598 (1999).
- [36] See Supplemental Material at <http://link.aps.org/supplemental/10.1103/PhysRevB.103.085115> for (1) pressure dependence of the transition energy of $^3A_{2g}(F) \rightarrow ^3T_{2g}(F)$ and $^3T_{1g}(F)$; (2) pressure dependence of the transition energy of $^3A_{2g}(F) \rightarrow ^1E_g(D)$, $^1T_{2g}(D)$ and $^3T_{1g}(P)$; (3) variation of the transition oscillator strength with pressure for transitions: $^3A_{2g}(F) \rightarrow ^3T_{2g}(F)$, $^3T_{1g}(F)$, $^1E_g(D)$, $^1T_{2g}(D)$ and $^3T_{1g}(P)$; and (4) single crystal of $KNiF_3$ at different pressures inside a diamond anvil cell.
- [37] G. Shen, Y. Wang, A. Dewaele, C. Wu, D. E. Fratanduono, J. Eggert, S. Klotz, K. F. Dziubek, P. Loubeyre, O. V. Fat'yanov, P. D. Asimow, T. Mashimo, R. M. M. Wentzcovitch, and other members of the IPPS task group, *High Press. Res.* **40**, 299 (2020).
- [38] J. A. Barreda-Argüeso and F. Rodríguez, US Patent No. PCT/ES2014/000049 (2014).
- [39] J. Ferguson, H. J. Guggenheim, and D. L. Wood, *J. Chem. Phys.* **40**, 822 (1964).
- [40] J. Ferguson and H. J. Guggenheim, *J. Chem. Phys.* **44**, 1095 (1966).

- [41] J. Grimm, O. S. Wenger, and H.U. Güdel, *J. Lumin.* **102-103**, 380 (2003); C. Lin, C. Liu, Z. Zhao, L. Li, C. Bocker, and C. Rüssel, *Opt. Lett.* **40**, 5263 (2015).
- [42] R. Alcala, J. Casas González, B. Villacampa, and P. J. Alonso, *J. Lumin.* **48-49**, 569 (1991).
- [43] B. Villacampa, R. Cases, V. M. Orera, and R. Alcala, *J. Phys. Chem. Solids* **55**, 263 (1994).
- [44] G. Wu and R. Hoppe, *Z. Anorg. Allg. Chem.* **514**, 92 (1984).
- [45] J. A. Barreda-Argüeso, L. Nataf, F. Aguado, I. Hernández, J. González, A. Otero-de-la-Roza, V. Luaña, Y. Jia, C. Jin, B. Kim, K. Kim, B. I. Min, W. Heribert, A. P. Jephcoat, and F. Rodríguez, *Sci. Rep.* **9**, 5448 (2019).
- [46] L. Nataf, J. A. Barreda-Argüeso, R. Valiente, J. González, and F. Rodríguez, *Phys. Rev. B* **89**, 115120 (2014).